


Core-halo boundary in a sheet beam model

Cite as: Phys. Plasmas **28**, 113103 (2021); <https://doi.org/10.1063/5.0068539>

Submitted: 25 August 2021 • Accepted: 26 October 2021 • Published Online: 09 November 2021

Antônio H. Carlan and  Renato Pakter



[View Online](#)



[Export Citation](#)



[CrossMark](#)

ARTICLES YOU MAY BE INTERESTED IN

[Theoretical foundations for the evanescent mode oscillator \(EMO\) as a high-efficiency source of millimeter-wave and terahertz radiations](#)

Physics of Plasmas **28**, 113104 (2021); <https://doi.org/10.1063/5.0068155>

[Parasitic excitation of fundamental-cyclotron-harmonic waves in high-harmonic gyrotrons](#)

Physics of Plasmas **28**, 113105 (2021); <https://doi.org/10.1063/5.0071351>

[Origin and structure of electromagnetic generator regions at the edge of the electron diffusion region](#)

Physics of Plasmas **28**, 112901 (2021); <https://doi.org/10.1063/5.0068317>



Physics of Plasmas
Features in Plasma Physics Webinars

Register Today!

Core-halo boundary in a sheet beam model

Cite as: Phys. Plasmas **28**, 113103 (2021); doi: [10.1063/5.0068539](https://doi.org/10.1063/5.0068539)

Submitted: 25 August 2021 · Accepted: 26 October 2021 ·

Published Online: 9 November 2021




View Online



Export Citation



CrossMark

Antônio H. Carlan, Jr. and Renato Pakter^{a)} 

AFFILIATIONS

Instituto de Física, Universidade Federal do Rio Grande do Sul, Caixa Postal 15051, 91501-970 Porto Alegre, RS, Brazil

^{a)}Author to whom correspondence should be addressed: pakter@if.ufrgs.br

ABSTRACT

In this paper, halo formation in a sheet beam model is investigated. Special attention is given to the core-halo boundary. In particular, a theory to determine the final stationary state achieved by an initially mismatched beam is developed. An interesting property of the theory is that it clearly separates the core and the halo portions of the distribution. Self-consistent numerical simulations are employed to obtain particle distributions for the sheet beam stationary state. Using the maximum Laplacian criteria, the core-halo boundary is evaluated from the numerical data for both one-dimensional projections of the beam distribution as well as the full multi-dimensional phase space. The results are compared to those predicted by the theory.

Published under an exclusive license by AIP Publishing. <https://doi.org/10.1063/5.0068539>

I. INTRODUCTION

Different applications, such as heavy ion fusion, neutron irradiation, tritium production, and nuclear waste transmutation, have been pushing the need for particle accelerators capable of dealing with beams with increasing intensities and power. In these devices, the space charge forces play a dominant role leading to the onset of nonlinear effects that may be detrimental to the beam quality.^{1–7} In particular, halos are a major cause for particle loss and wall activation. In general, halos are produced when some particles gain energy at the expense of the collective self-field perturbations produced by mismatched oscillations or distribution inhomogeneities in the beam.^{1,2,8–13}

Although the presence of halos is generally clearly noticeable by a direct visual analysis of the particles distribution, it is of particular interest to derive a more quantitative way to measure it. This allows, for instance, to optimize the accelerator design by taking into account the halo dynamics.^{14,15} Different methods have been proposed to define the halo.^{16–19} Here, we will give special attention to that described in Ref. 18 because it can be readily calculated from the beam distribution and it provides a clear definition of the boundary between the core and halo. The key idea is that the boundary is located where the Laplacian of the particle distribution function is maximum. An important point, however, is that since the distribution function obtained from experiments and numerical simulations are noisy, their derivatives have to be evaluated with caution otherwise the noise will be largely amplified. Hence, it was proposed the use of *sliding derivatives* obtained by averaging them over different ranges around each point.^{18,20,21}

In this paper, we investigate the halo formation in a sheet beam model.^{22–24} This model is considered because, despite its simplicity as compared to higher-dimensional models of beams in particle accelerators, it provides a useful framework to study the role of the space-charge. Special attention is given to the core-halo boundary. In particular, we develop a theory to determine the final stationary state achieved by an initially mismatched beam. The theory is analogous to those already successfully applied to 2D continuous beams,^{25,26} 3D bunched beams,²⁷ and other long-range interacting systems, such as self-gravitating systems, spin models, and vortex systems.^{28–33} An interesting property of the theory is that it clearly separates the core and the halo portions of the distribution. From self-consistent numerical simulations, we obtain particle distributions for the sheet beam stationary state which are used to determine the halo boundary using the maximum Laplacian criteria. These results are tested against the theory. We start by considering one-dimensional projections of the beam distribution as in Refs. 18 and 20. However, since a detailed description of the halo requires its knowledge in the full phase-space, we also extend the method to higher dimensional spaces. This is particularly relevant if one takes into account that present experimental methods allow for a full multi-dimensional beam phase-space measurement.^{34–39}

The paper is organized as follows. In Sec. II, we present the sheet beam model and the equations that dictate its dynamics. In Sec. III, we use the envelope equation to investigate mismatched beam oscillations and determine the halo size from a particle-core analysis. The theory that describes the final stationary state is presented in Sec. IV. In Sec. V, the numerical simulation method is described and some of its

results are discussed. In Sec. VI, the maximum Laplacian criterion is used to determine the core-halo boundary from particle distributions numerically obtained and the results are compared with the theory. Finally, in Sec. VII we present our conclusions.

II. MODEL

Let us consider an intense beam of particles of mass m and charge q that are propagating along the z axis with a constant axial velocity $\beta_b c$, where c is the speed of light *in vacuo*. In accordance with the sheet model,^{22–24} we assume that the beam is uniform in the y and z directions, such that its evolution is completely described by the distribution function $f(x, p, s)$, where p is the canonical momentum conjugate to the coordinate x and $s = \beta_b c t$ plays the role of time. We also take into account a uniform linear focusing force acting on the beam in the x direction in order to compensate for the space charge and grounded conducting plates located at $x = \pm L$.

Given the collisionless nature of the self-beam interaction, the particle distribution function $f(x, p, s)$ evolves according to the Vlasov equation,^{5,23,24}

$$\frac{\partial f}{\partial s} + \frac{\partial H}{\partial p} \frac{\partial f}{\partial x} - \frac{\partial H}{\partial x} \frac{\partial f}{\partial p} = 0, \quad (1)$$

where H is the single-particle Hamiltonian,

$$H = \frac{1}{2} p^2 + \frac{1}{2} \kappa x^2 + \psi(x, s). \quad (2)$$

Here, κ is the focusing strength parameter and $\psi(x) = q\phi(x)/m\gamma_b^3\beta_b^2c^2$ is a normalized potential that is determined by the one-dimensional Poisson equation,

$$\frac{\partial^2 \psi}{\partial x^2} = -2P n(x, s), \quad (3)$$

subject to the boundary conditions $\psi(x = \pm L, s) = 0$, where $\phi(x, s)$ is the electrostatic potential, $P = q^2 N / 2\epsilon_0 m\gamma_b^3\beta_b^2c^2$ is the sheet-beam perveance, $\gamma_b = (1 - \beta_b^2)^{-1/2}$ is the relativistic mass factor, ϵ_0 is the vacuum permittivity,

$$n(x, s) = \int_{-\infty}^{\infty} f(x, p, s) dp, \quad (4)$$

is the beam particle density, and $N = \int_{-L}^L n(x, s) dx = \text{const.}$ is the number of particles per unit surface area.

Given an initial distribution at $s = 0$, the Vlasov–Poisson system of Eqs. (1)–(4) completely describes the self-consistent nonlinear evolution for the sheet beam. In particular, we will consider initial distributions of the form

$$f_0(x, p) = \frac{N}{4x_0 p_0} \Theta(x_0 - |x|) \Theta(p_0 - |p|), \quad (5)$$

where Θ is the Heaviside step function. Equation (5) corresponds to an uncorrelated whaterbag distribution in the phase-space variables, where particles are uniformly distributed in the region $-x_0 \leq x \leq x_0$ and $-p_0 \leq p \leq p_0$. It is worth noting that since both the initial condition in Eq. (5) and the external focusing force are symmetric with respect to $x = 0$ and $p = 0$, the beam distribution will preserve this symmetry throughout the evolution.

III. MISMATCHED BEAM AND HALO SIZE

Depending on the parameters of the injected beam and the external field, one would expect that there may be some instances where an overall balance between focusing and defocusing forces is found. In such cases, the transverse size of the beam in the x direction is expected to present very little variations along the transport. On the other hand, if there is a sizeable mismatch between these competing forces, large amplitude beam oscillations occur.

To investigate this issue, it is convenient to introduce a beam envelope,

$$x_b(s) = \sqrt{3\langle x^2 \rangle}, \quad (6)$$

where $\langle \cdots \rangle \equiv \int \cdots f(x, p, s) dx dp$ is the average over beam distribution. This quantity is an rms measure of the beam transverse size. Taking two derivatives of x_b with respect to s and assuming that the beam particles remain uniformly distributed in the region $-x_b(s) \leq x \leq x_b(s)$ for all s , we obtain the envelope equation,^{22,24}

$$\frac{d^2 x_b}{ds^2} = -\kappa x_b + P + \frac{\varepsilon^2(s)}{x_b^3}, \quad (7)$$

where $\varepsilon(s) = 3\sqrt{\langle x^2 \rangle \langle p^2 \rangle - \langle xp \rangle^2}$ is the sheet-beam emittance. Considering the initial condition in Eq. (5), we obtain that at $s = 0$ the envelope is $x_b = x_0$, its derivative is $dx_b/ds = 0$, and the emittance is $\varepsilon_0 = x_0 p_0$. Hence, if the beam is injected with $x_0 = x_{bm}$, where

$$-\kappa x_{bm} + P + \frac{\varepsilon_0^2}{x_{bm}^3} = 0, \quad (8)$$

then the overall force on the envelope vanishes and beam oscillations are not expected. Although Eq. (8) is a fourth-order polynomial equation for x_{bm} , it only presents a single physical solution (real and positive root) which corresponds to the matched beam envelope.

For mismatched cases, when $x_0 \neq x_{bm}$, the envelope will start to oscillate. These oscillations resonate with some of the beam particles, exciting them to higher energy regions of the phase-space, forming the halo.² This will eventually lead to emittance growth and a damping of the envelope oscillations.¹⁰ The halo particles that gain more energy are those that are excited in the beginning of the process when the envelope oscillation amplitude is larger and there is little variation of the emittance. Therefore, to estimate the outermost size of the halo we can investigate the dynamics of test particles interacting with a core whose envelope oscillates according to Eq. (7) with a constant emittance.⁸ This is the, so-called, particle-core model. Assuming that the core is uniformly distributed, the equation for the evolution of the test particle is

$$\frac{d^2 x}{ds^2} + \kappa x = \begin{cases} P x / x_b(s), & \text{if } |x| \leq x_b(s), \\ P x / |x|, & \text{if } |x| > x_b(s), \end{cases} \quad (9)$$

where $x_b(s)$ is obtained from Eq. (7) with $\varepsilon(s) = \varepsilon_0 = \text{const.}$ An inspection on Eqs. (7) and (9) with $\varepsilon(s) = \varepsilon_0$ reveals that if we scale x_b and x to $(\varepsilon_0^2/\kappa)^{1/4}$ and s to $\kappa^{-1/2}$, we are left with a single parameter $\Pi = P/(\kappa^3 \varepsilon_0^2)^{1/4}$, which measures the relative strength of space-charge, focusing, and emittance effects. In Fig. 1, we present a stroboscopic plot of the test-particle phase-space obtained for $x_0 = 1.5 x_{bm}$ and $\Pi = 1.0$. The thick red dots correspond to a separatrix that is responsible for the resonant excitation of particles just outside the

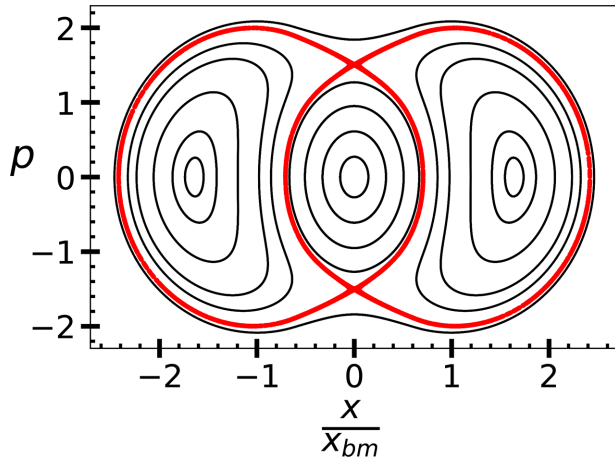


FIG. 1. Stroboscopic plot of test-particles phase-space for $x_0 = 1.5 x_{bm}$ and $\Pi = 1.0$. We numerically integrate Eq. (9) for different initial conditions along with Eq. (7) and plot the test particles trajectories each time the envelope reaches a minimum. The thick red dots correspond to the separatrix that excites particles to the halo. The maximum x along the separatrix corresponds to the halo size, $x_h = 2.42 x_{bm}$.

beam core.² The maximum x along the separatrix gives us an estimate of the halo size as $x_h = 2.42 x_{bm}$.

Using the method described above, we can determine the halo size for different values of the system parameters. In Fig. 2, the symbols show the results obtained for the halo size normalized to the matched beam envelope for different values of Π . Based on a dimensional analysis, it has been proposed that x_h/x_{bm} should be independent of Π for a fixed mismatch amplitude x_0/x_{bm} .⁸ As a matter of fact, this has been verified for unbunched spherically symmetric beams.²⁷ In the present case, we notice that there is a certain dependence of x_h/x_{bm} on Π , which can be well described by the line $x_h/x_{bm} = 2.5 - 0.074 \Pi$. This result will be used in Sec. IV to determine the final stationary state.

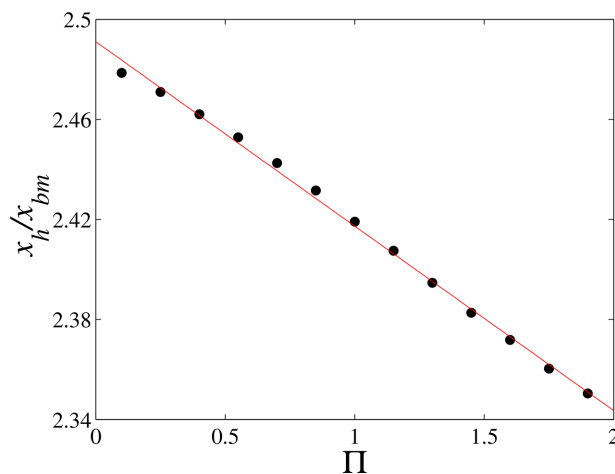


FIG. 2. Halo size x_h normalized to the matched envelope x_{bm} as a function of the parameter Π for $x_0 = 1.5 x_{bm}$. The symbols are the results obtained using the test particle analysis. The line corresponds to a linear regression of the results.

IV. THEORETICAL PREDICTION OF THE BEAM STATIONARY STATE

As long as the envelope of an initially mismatched beam is oscillating, halo is being formed by the resonant excitation of some of the beam particles. Due to conservation of energy, as the halo particles gain energy, those that remain in the core have to lose it. This process continues until the core particles reach their lowest energy configuration on the phase-space. Because the beam evolution is dictated by the Vlasov Eq. (1) and, therefore, incompressible in the phase-space, the core particles cannot all condensate to the lowest energy point. Instead, analogous to a fully degenerate Fermi gas, they populate all the lower energy states available with the maximum density allowed up to a certain Fermi energy ϵ_F . Given the initial condition in Eq. (5), the maximum density allowed corresponds to the initial density $N/4x_0p_0$. As for the halo, we assume that in the stationary state its particles are uniformly distributed in energy from ϵ_F to the energy of the particle that reaches the halo size x_h obtained in Sec. III. Hence, we write the distribution function of the stationary state as

$$f_s(x, p) = \frac{N}{4x_0p_0} \begin{cases} 1, & \text{if } H(x, p) \leq \epsilon_F, \\ \chi, & \text{if } \epsilon_F < H(x, p) < \epsilon_h, \end{cases} \quad (10)$$

where $H(x, p)$ is the single-particle Hamiltonian in Eq. (2), χ is the relative halo density, and $\epsilon_h = \kappa x_h^2/2 + P(L - x_h)$ is the energy of the particle that reaches the halo size x_h . Note that once the beam has reached the stationary state, $H(x, p)$ becomes a single-particle constant of motion. Thence, $f_s(x, p)$ is a true Vlasov equilibrium because it only depends on the phase-space coordinates through $H(x, p)$. In Eq. (10), both ϵ_F and χ are yet unknown. We use the conservation of particles and beam energy to determine their values.

Integrating Eq. (10) with respect to the momentum p to determine the beam particle density and substituting this result in the Poisson Eq. (3), we obtain a closed nonlinear equation for the normalized potential,

$$\frac{\partial^2 \psi}{\partial x^2} = -\frac{NP}{x_0p_0} \left[(1 - \chi) \sqrt{2\epsilon_F - \kappa x^2 - 2\psi(x)} + \chi \sqrt{2\epsilon_h - \kappa x^2 - 2\psi(x)} \right], \quad (11)$$

where the contribution of the square-roots are to be considered only when their arguments are non-negative. For given values of the system parameters and ϵ_F and χ , we numerically solve Eq. (11) with the prescribed boundary conditions using a shooting method. We then use a Newton-Raphson method to determine the values of ϵ_F and χ that lead to the conservation of particles and energy,

$$\int f_s(x, p) dx dp = N, \quad (12)$$

$$\int \left[\frac{p^2 + \kappa x^2 + \psi(x)}{2} \right] f_s(x, p) dx dp = E_0, \quad (13)$$

where $E_0 = N[p_0^2 + \kappa x_0^2 + P(3L - 2x_0)]/6$ is the energy of the initial distribution given by Eq. (5). Following this procedure, we can obtain a fully self-consistent prediction for the stationary state achieved by the beam. Examples of such states will be presented and compared to the results from numerical simulation in Sec. V.

V. NUMERICAL SIMULATIONS

To perform self-consistent numerical simulations for the evolution of sheet beams, we consider a *large* number $N_s = 20\,000$ of charge sheets located at phase-space positions $x_i(s)$ and $p_i(s)$, $i = 1, \dots, N_s$, which are initially distributed according to Eq. (5). With the aid of Green's functions, we can determine the interaction potential between two different sheets.⁴⁰ The acceleration of the i th simulated sheet is found to be

$$\frac{d^2 x_i}{ds^2} = -\kappa x_i + P \left(\frac{2N_{<}}{N_s} + \frac{\langle x \rangle}{L} - 1 \right), \quad (14)$$

where $N_{<}$ is the sum of charge sheets located to the left of the i th sheet [$x_j(s) < x_i(s)$] and $\langle x \rangle$ is the position of the centroid of the distribution. In our simulations, we make use of initial conditions that are symmetric with respect to $x = 0$ and $p = 0$, such that $\langle x \rangle = 0$ for all s .

Let us first consider a simulation for the case with $x_0 = 1.5 x_{bm}$ and $\Pi = 1.0$. In Fig. 3, it is shown the evolution obtained for the beam emittance. We observe that ε rapidly increases from its initial value ε_0 and eventually reaches a nearly constant value of $\varepsilon \approx 1.52\varepsilon_0$. Although there is still a residual oscillation due to the finite number of particles, the result in Fig. 3 indicates that the stationary state has already been achieved for $s = 5.0 \times 10^4$. In Fig. 4 we present the distribution in phase-space. In panel (a), it is shown the initial distribution of charge sheets that corresponds to the waterbag. In panel (b), where the stationary state is shown, we can clearly see the formation of the core-halo structure with a lower density distribution of particles surrounding a higher density one. We also include in panel (b) the iso-energy curves that correspond to $H(x, p) = \varepsilon_F$ (red curve) and $H(x, p) = \varepsilon_h$ (blue curve). In agreement with the theory, we note that the higher density core is contained in the phase-space region with $H(x, p) < \varepsilon_F$, whereas the lower density halo is found for $\varepsilon_F < H(x, p) < \varepsilon_h$.

To further test the theory, we have also run simulations for other values of the parameter Π . In general, a good agreement was found. To illustrate this, in Fig. 5 we compare the emittance growth predicted

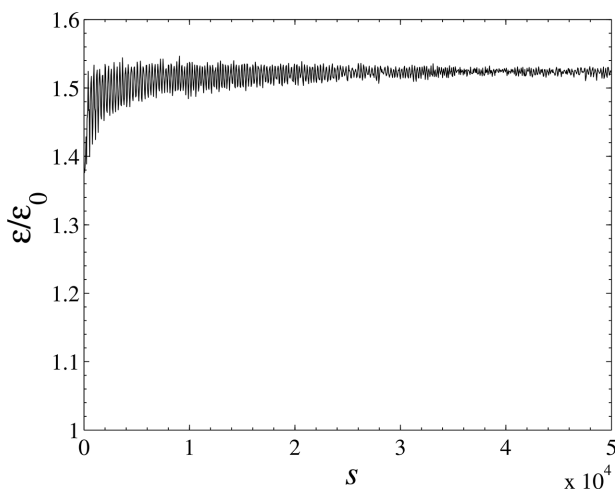


FIG. 3. Emittance evolution obtained from a numerical simulation with $N_s = 20\,000$ charge sheets for $x_0 = 1.5 x_{bm}$ and $\Pi = 1.0$.

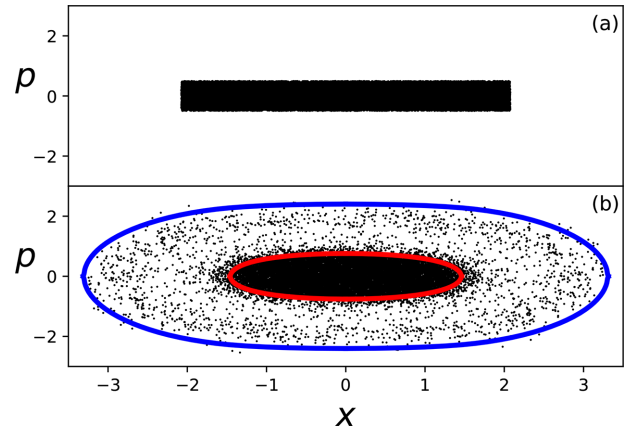


FIG. 4. Particles distribution in phase-space for a simulation with $N_s = 20\,000$, $x_0 = 1.5 x_{bm}$, and $\Pi = 1.0$. In (a) it is shown the initial condition and, in (b), the stationary state. The curves in panel (b) correspond to $H(x, p) = \varepsilon_F$ (red) and $H(x, p) = \varepsilon_h$ (blue) as obtained from the theory. They delimit the core and the halo, respectively.

by the theory (red curve) and that obtained from the simulations (black symbols). In all the cases, the relative error was less than 1%.

VI. CORE-HALO BOUNDARY

As discussed in the Introduction, the determination of the boundary between core and halo is of great relevance. From the point of view of the theory described in Sec. IV, it is not difficult to see that this boundary is related to the Fermi energy ε_F that sets the maximum energy that a core particle can achieve. In particular, if we concentrate on the coordinate x , the boundary corresponds to the point x_c that satisfies $H(x = x_c, p = 0) = \varepsilon_F$. This is the maximum coordinate reached by a core particle and corresponds to the rightmost tip of the red curve in Fig. 4(b). In Fig. 6, the red solid curve shows the values of x_c obtained for $x_0 = 1.5 x_{bm}$ as the parameter Π is varied.

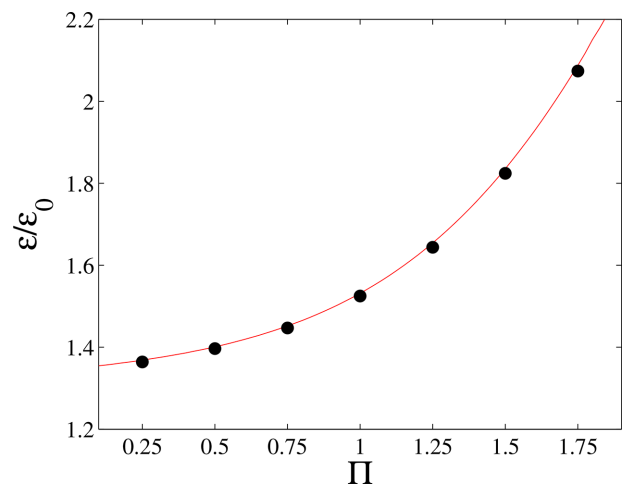


FIG. 5. Comparison between the emittance growth obtained from the numerical simulations (black symbols) and the theory (red curve).

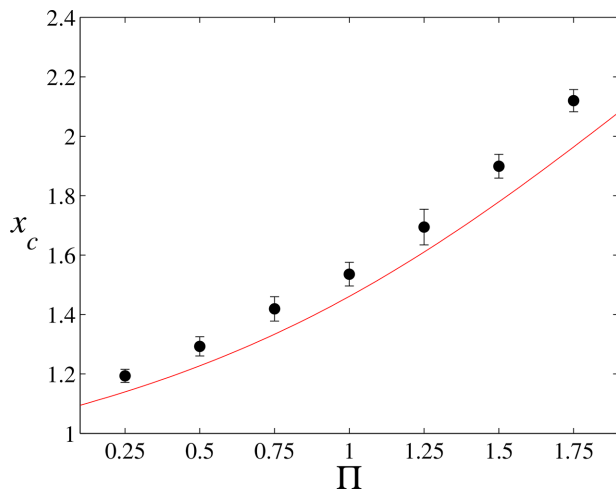


FIG. 6. Core-halo boundary x_c as a function of the parameter Π for $x_0 = 1.5 x_{bm}$. The solid red curve corresponds to the values obtained from the theory presented in Sec. IV using $H(x = x_c, p = 0) = \varepsilon_F$. The symbols were calculated using the method proposed in Refs. 18 and 20 on numerically obtained particle distributions. To measure the effect of fluctuations due to the finite number of particles we show the average and standard error of x_c calculated at 20 different longitudinal positions s after the stationary states were attained.

On the other hand, for particle distributions obtained from experiments and simulations the determination of the core-halo boundary is generally not so direct. Nevertheless, in Ref. 18 it was proposed that the boundary is located where the Laplacian of the particle density is maximum. In the present case of the 1D sheet beam model, this corresponds to the maximum of the second derivative of $n(x)$. In order to prevent the noise amplification generated by the numerical derivatives, it was suggested the use of *sliding derivatives* obtained by averaging them over different ranges around each point.^{18,20} We apply the proposed method to calculate the core-halo boundary x_c from stationary state distributions obtained from the numerical simulations. As in Ref. 18, we computed $n(x)$ distributing the particles over 200 bins and performed the sliding derivatives averaging over 10 bins. The position of the maximum of d^2n/dx^2 was taken as x_c . The results are represented by the symbols with error bars in Fig. 6. We notice that there is a reasonably good agreement with the theoretically predicted results and that the fluctuation amplitudes around the average are relatively small, indicating the validity and robustness of the method. We also notice that x_c obtained from the simulation tends to be higher than the theoretical one. This is possibly caused by the finite number of particles in the simulation that tend to blurry the core-halo boundary as some core particles *diffuse* to the halo region.

Although the core-halo boundary along one given coordinate already provides some relevant information, it is clear that to fully characterize the core-halo structure one needs to determine its boundary in the full multidimensional phase-space. This is noticeable, for instance, in Fig. 4(b) where one notices that a reasonable fraction of the halo particles are found for $|x| < x_c$ as they spread out up to large values of p . The *real* core-halo boundary corresponds to the curve $H(x, p) = \varepsilon_F$ (red curve in the figure). The question is, can we adequately determine this curve from numerically obtained particle distributions using the maximum Laplacian method? To answer this, we

use the results from our numerical simulations to obtain $f(x, p)$ by distributing the particles over a 200×200 grid. To improve the statistics, we have averaged the distribution over 20 different longitudinal positions s after the stationary states had been achieved. Using the sliding derivatives in both coordinate and momentum, we calculated $\nabla^2 f = \partial^2 f / \partial p^2 + \partial^2 f / \partial x^2$. The result is shown in Fig. 7. The shape resembles that of a volcano. It is then expected that its rim should describe the core-halo boundary. Because the *height* largely varies along the rim, it is not suitably described by an isocurve of $\nabla^2 f$. Hence, to determine its position we adopt the following procedure. We separate the phase-space in different sectors of the angle $\theta = \tan^{-1}(p/x)$. The sectors are uniformly distributed between 0 and 2π . For each sector, we determine the position of the maximum of $\nabla^2 f$. Joining these points with straight lines, we obtain a closed curve that represents the core-halo boundary. The result is presented by the blue curve in Fig. 8. For the sake of comparison, we also show in the figure the particle distribution obtained from the simulation and the theoretically predicted curve. Overall, a very good agreement is found.

VII. CONCLUSIONS

We investigated the halo formation in a sheet beam model. Special attention was given to the core-halo boundary. In particular, a theory was developed to determine the final stationary state achieved by an initially mismatched beam. An interesting property of the theory is that it clearly separates the core and the halo portions of the distribution. From self-consistent numerical simulations, we obtained particle distributions for the sheet beam stationary state. They were used to determine the halo boundary using the maximum Laplacian criteria. We first considered one-dimensional projections of the beam distribution. Nevertheless, since a detailed description of the halo requires its knowledge in the full phase-space, we extended the method to higher dimensional spaces. This allowed us to evaluate the curve that corresponds to the core-halo boundary in the sheet beam phase-space from numerical data. An overall good agreement was found with the results predicted by the theory. All the results presented in the paper consider a fixed mismatch amplitude $x_0/x_{bm} = 1.5$. However, we have also

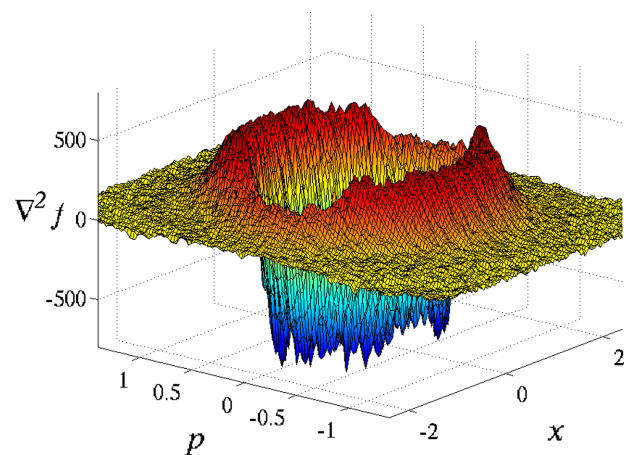


FIG. 7. Three-dimensional representation of $\nabla^2 f(x, p)$. The particle distribution function $f(x, p)$ was obtained from a numerical simulation with $x_0 = 1.5 x_{bm}$ and $\Pi = 1.0$.

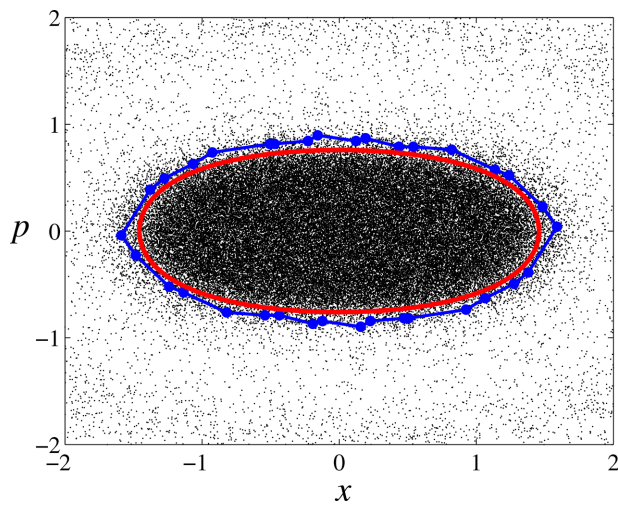


FIG. 8. Core-halo boundary in phase-space. The blue curve with symbols is the result from the analysis of the numerical simulation data using the maximum Laplacian method. Particularly, the symbols correspond to the positions of the maxima of $\nabla^2 f$ in each sector in θ . The red curve is the theoretically predicted one, $H(x, p) = \varepsilon_F$. The particles positions in phase-space are also presented (black points).

investigated other values of the parameter in the range $1.2 \leq x_0/x_{bm} \leq 2.0$ and found the agreement between theory and simulation to be similar to those presented here. The method applied here to calculate the core-halo boundary in the two-dimensional phase-space of a sheet beam can be straightforwardly extended to higher dimensional phase-spaces of more realistic beams. Namely, for a d -dimensional phase-space, the hypersurface of dimension $d - 1$ that represents the core-halo boundary would be obtained by joining the points of maxima of the Laplacian of the particle distribution $f(\mathbf{r}, \mathbf{p})$ for neighboring sections of a hyper-solid angle in the phase-space.

ACKNOWLEDGMENTS

This work was supported by CNPq, Brazil.

AUTHOR DECLARATIONS

Conflict of Interest

The authors have no conflicts to disclose.

DATA AVAILABILITY

The data that support the findings of this study are available within the article and its supplementary material.

REFERENCES

- ¹A. Cuchetti, M. Reiser, and T. Wangler, in *Proceedings of the Invited Papers, 14th Particle Accelerator Conference, San Francisco, California*, edited by L. Lizama and J. Chew (IEEE, New York, 1991), Vol. 1, p. 251.
- ²R. L. Gluckstern, *Phys. Rev. Lett.* **73**, 1247 (1994).
- ³C. Chen and R. C. Davidson, *Phys. Rev. Lett.* **72**, 2195 (1994).
- ⁴R. Pakter and F. B. Rizzato, *Phys. Rev. Lett.* **87**, 044801 (2001).
- ⁵R. C. Davidson and H. Qin, *Physics of Intense Charged Particle Beams in High Energy Accelerators* (World Scientific, New York, 2001).
- ⁶R. Pakter and F. B. Rizzato, *Phys. Rev. E* **65**, 056503 (2002).
- ⁷W. Simeoni, Jr., F. B. Rizzato, and R. Pakter, *Phys. Plasmas* **13**, 063104 (2006).
- ⁸T. P. Wangler, K. R. Crandall, R. Ryne, and T. S. Wang, *Phys. Rev. Spec. Top. Accel. Beams* **1**, 084201 (1998).
- ⁹C. Chen and R. Pakter, *Phys. Plasmas* **7**, 2203 (2000).
- ¹⁰K. Fiuza, F. B. Rizzato, and R. Pakter, *Phys. Plasmas* **13**, 023101 (2006).
- ¹¹F. B. Rizzato, R. Pakter, and Y. Levin, *Phys. Plasmas* **14**, 110701 (2007).
- ¹²R. P. Nunes, R. Pakter, and F. B. Rizzato, *Phys. Plasmas* **14**, 023104 (2007).
- ¹³E. G. Souza, A. Endler, R. Pakter, F. B. Rizzato, and R. P. Nunes, *Appl. Phys. Lett.* **96**, 141503 (2010).
- ¹⁴H. Li, Z. Wang, Y. Lu, S. Wang, K. Zhu, F. Zhu, S. Peng, Z. Guo, Q. Tan, and S. Liu, *J. Instrum.* **15**, P09036 (2020).
- ¹⁵P. A. P. Nghiem, N. Chauvin, M. Comunian, O. Delferriere, R. Duperrier, A. Mosnier, C. Oliver, W. Simeoni, Jr., and D. Uriot, *Laser Part. Beams* **32**, 109 (2014).
- ¹⁶C. K. Allen and T. P. Wangler, *Phys. Rev. Spec. Top. Accel. Beams* **5**, 124202 (2002).
- ¹⁷M. A. Dorf, R. C. Davidson, and E. A. Startsev, *Phys. Plasmas* **18**, 043109 (2011).
- ¹⁸P. A. P. Nghiem, N. Chauvin, W. Simeoni, and D. Uriot, *Appl. Phys. Lett.* **104**, 074109 (2014).
- ¹⁹R. P. Nunes and W. Simeoni, Jr., *J. Plasma Phys.* **84**, 905840207 (2018).
- ²⁰P. A. P. Nghiem, M. Valette, N. Chauvin, N. Pichoff, and D. Uriot, *Phys. Plasmas* **22**, 083115 (2015).
- ²¹M. Valette and P. A. P. Nghiem, in *Proceedings of the 6th International Particle Accelerator Conference (IPAC'15)*, Richmond, VA (IPAC, 2015), p. 99.
- ²²R. C. Davidson, H. Qin, S. I. Tzenov, and E. A. Startsev, *Phys. Rev. Spec. Top. Accel. Beams* **5**, 084402 (2002).
- ²³E. A. Startsev and R. C. Davidson, *Phys. Rev. Spec. Top. Accel. Beams* **6**, 044401 (2003).
- ²⁴S. M. Lund, A. Friedman, and G. Bazouin, *Phys. Rev. Spec. Top. Accel. Beams* **14**, 054201 (2011).
- ²⁵Y. Levin, R. Pakter, and T. N. Teles, *Phys. Rev. Lett.* **100**, 040604 (2008).
- ²⁶T. N. Teles, R. Pakter, and Y. Levin, *Phys. Rev. Spec. Top. Accel. Beams* **13**, 114202 (2010).
- ²⁷T. M. Corrêa da Silva, R. Pakter, F. B. Rizzato, and Y. Levin, *Phys. Plasmas* **22**, 023102 (2015).
- ²⁸T. N. Teles, Y. Levin, R. Pakter, and F. B. Rizzato, *J. Stat. Mech.* **2010**, P05007.
- ²⁹T. N. Teles, Y. Levin, and R. Pakter, *Mon. Not. R. Astron. Soc.* **417**, L21 (2011).
- ³⁰R. Pakter and Y. Levin, *Phys. Rev. Lett.* **106**, 200603 (2011).
- ³¹Y. Levin and R. Pakter, *Phys. Rev. Lett.* **107**, 088901 (2011).
- ³²Y. Levin, R. Pakter, F. B. Rizzato, T. N. Teles, and F. P. C. Benetti, *Phys. Rep.* **535**(1), 1–60 (2014).
- ³³R. Pakter and Y. Levin, *Phys. Rev. Lett.* **121**, 020602 (2018).
- ³⁴V. Yakimenko, M. Babzien, I. Ben-Zvi, R. Malone, and X.-J. Wang, *Phys. Rev. Spec. Top. Accel. Beams* **6**, 122801 (2003).
- ³⁵F. Zhou, A. Kabel, J. Rosenzweig, R. Agustsson, G. Andonian, D. Cline, A. Murokh, and V. Yakimenko, *Phys. Rev. ST Accel. Beams* **9**, 114201 (2006).
- ³⁶D. Stratakis, K. Tian, R. A. Kishek, I. Haber, M. Reiser, and P. G. O'Shea, *Phys. Plasmas* **14**, 120703 (2007).
- ³⁷D. Stratakis, R. A. Kishek, I. Haber, S. Bernal, M. Reiser, and P. G. O'Shea, *Phys. Rev. ST Accel. Beams* **12**, 064201 (2009).
- ³⁸D. Stratakis, R. A. Kishek, S. Bernal, R. B. Fiorito, I. Haber, M. Reiser, P. G. O'Shea, K. Tian, and J. C. T. Thangaraj, *Phys. Plasmas* **17**, 056701 (2010).
- ³⁹B. Cathey, S. Cousineau, A. Aleksandrov, and A. Zhukov, *Phys. Rev. Lett.* **121**, 064804 (2018).
- ⁴⁰F. B. Rizzato, R. Pakter, and Y. Levin, *Phys. Rev. E* **80**, 021109 (2009).